Published in the Proceedings of the 16th International Aluminum Alloys Conference (ICAA16) 2018
ISBN: 978-1-926872-41-4
by the Canadian Institute of Mining, Metallurgy & Petroleum

MECHANICAL BEHAVIOUR AND CONSTITUTIVE MODELING OF AlSi10Mg-200°C ADDITIVELY MANUFACTURED THROUGH DIRECT METAL LASER SINTERING

C. K. Baxter[1], E. D. Cyr[1], A. Odeshi[2], and M. Mohammadi[1]

[1] *Marine Additive Manufacturing Centre of Excellence, University of New Brunswick, Fredericton, New Brunswick, Canada*

[2] *Department of Mechanical Engineering, University of Saskatchewan, Saskatoon, SK, Canada*

ABSTRACT

Metal additive manufacturing has been a revolutionary step in designing new complex shapes with faster and cleaner building capacity in comparison to subtractive manufacturing processes. The ability to print lightweight alloys such as aluminum has made metal 3D printing attractive to different industrial sector from aerospace to energy and bioengineering. Of particular interest in this study, are the mechanical and microstructural properties of AlSi10Mg-200°C alloys. In this project, samples were 3D-printed in horizontal direction using an EOS M290 machine by Direct Metal Laser Sintering (DMLS) technique. Uniaxial tensile tests and high strain-rate impact e tests were carried out to investigate the mechanical properties and to study the repeatability of the process. A constitutive model is developed to predict the results of the mechanical tests at varying strain rates to better understand the high strain-rate behaviour of these alloys. Using optical microscopy, features such as scan tracks and melt pools within the AlSi10Mg-200°C samples were observed, and the microstructure was observed to be homogenous. The previously listed tests were compared to the results obtained for similar cast alloy counterpart, i.e. A360.0.

KEYWORDS

Additive manufacturing, AlSi10Mg, Direct metal laser sintering, Mechanical properties

INTRODUCTION

A relatively new way of manufacturing parts is on the increase as rapid prototyping becomes increasingly popular throughout the world. Additive manufacturing is a process which, given a 3D model, uses metallic material in powder form to build a part layer by layer until completion (Gu, Meiners, Wissenbach, & Poprawe, 2013). This way of rapid prototyping is very attractive in comparison to other possibilities because of its ability to accommodate complex design and geometries. Conventional manufacturing methods have limitations when it comes to complex geometries, but additive manufacturing allows for increased design flexibilities while maintaining a light and stable final product (Murr et al., 2012). It also allows for a reasonable cost, especially for small batch sizes that would otherwise be extremely expensive.

The samples prepared for this study were additively manufactured using an EOS M290 machine through direct metal laser sintering (DMLS) technique (Metal Solutions, 2014). The laser sintering process starts by adding a thin layer of the powdered material to the building platform. Based on the input from the 3D model, the laser fuses the powder at the points specified for that particular layer within the model. The building platform is then lowered exactly the height of one layer, a new powder layer is applied and the process is repeated so that each individual layer is fused together to produce the final part (Herzog, Seyda, Wycisk, & Emmelmann, 2016; Zinoviev, Zinovieva, Ploshikhin, Roimanova, & Balokhonov, 2016; Herderick, 2011). The thickness of the layers can vary, depending on the powder size and the base material, 3D printing technique, and specific application.

Additively manufactured aluminum alloy AlSi10Mg-200ºC, which its conventional counterpart A360.0 that is a widely used casting alloy, is studied and reported in this paper. This aluminum alloy has good weldability, hardenability, and high thermal conductivity (Thijs, Kempen, Kruth, & Humbeeck, 2012). Such an alloy is likely to gain increasing popularity as choice materials in additive manufacturing due to increasing demand for lightweight materials in the industry

Of particular interest in this study is a powder bed fusion technique called, Direct Metal Laser sintering. In a powder bed system, powder is swept onto the work bed of the system from the powder bed using an arm, where either a laser or electron beam melts the powder into the desired form for that particular layer (Frazier, 2014). These layers are, depending on the machine, 20–100 μm thick. Next, the work bed is lowered the thickness of one layer and the arm then sweeps the powder from the raised powder bed over the existing melted layer. The powder layer is then melted according to its two-dimensional slice and the process is repeated (Carter, Martin, Withers, & Attallah, 2013).

One of the biggest shortcomings of the additive manufacturing process at this time as a relatively new manufacturing method is the lack of reliable work done to determine the mechanical properties of additively manufactured parts. Although the mechanical properties for one type of sample can be obtained through mechanical testing, it is not feasible to do mechanical testing on every part, which is to be manufactured. Mechanical testing was carried out to on horizontally printed AlSi10Mg same parts. In addition, the mechanical properties of the conventional and commercial as-cast alloy (A360.1), currently used in the industry, were determined. By producing a predictive model, which is calibrated and verified based on the obtained experimental data, less physical testing will be required, leading to less material wastage.

EXPERIMENTAL

Experimental Setup

Material

AlSi10Mg-200°C powder provided by EOS GMBH was used to 3D print all the samples studied in this paper. The chemical composition of the powder is listed in Table 1.

Table 1. Chemical composition of AlSi10Mg-200ºC virgin powder used in this study

Element	Si	Fe	Cu	Mn	Mg	Ti	Zn	Al
Weight (%)	10.08	0.16	0.001	0.002	0.35	0.001	0.002	Balance

EOS M290 machine was used to manufacture the samples. This machine utilizes a 400-W Yb-fiber laser and has a build volume of 250 mm × 250 mm × 325 mm (Metal Solutions, 2014). The machine is located in the Additive Metal Manufacturing Inc. facility in Concord, Ontario. Based on the recommendation provided by EOS GMBH, the building platform temperature was raised and held at 200°C to minimize the internal stresses and enhance the final geometries of the manufactured parts.

Experimental Procedure

Additively manufactured AlSi10Mg-200°C samples were used in this study. An Instron Model 1332 was used along with an 8500+ controller to perform tensile tests on the specimens. The impact tests at high strain rates was conducted using Split Hokinson pressure bar.

Since the DMLS method introduces a layer-by-layer manufacturing process, the final product may exhibit anisotropic behaviour. The mechanical properties of 3D printed metal samples are almost the same in the x-y plane (Manfredi et al., 2013); thus, only two directions: horizontal (xy) and vertical (z) are normally considered in mechanical testing of additively machines plates. In this study, only horizontal specimens were tested (Figure 1).

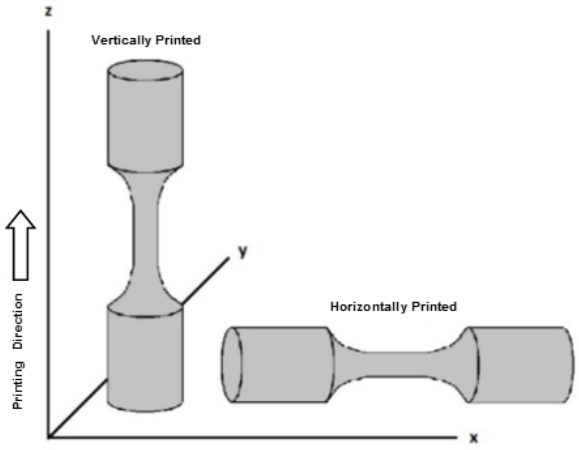

Figure 1. Orientation of horizontally and vertically printed samples

The horizontal tensile samples were originally 3D printed as cylindrical specimen with a length of 102 mm and a diameter of 12.47 mm. The tensile specimens were produced from this rods according to ASTM E8-15a Standard. The dimensions of the tensile test specimens are provided in Table 2.

Table 2. Dimensions for tensile test specimens

	Dimension (mm)
Gauge length (G)	24
Diameter (D)	6
Radius of fillet (R)	6
Length of reduced section (A)	30

For the tensile tests, standard aluminum samples were used first to ensure the correctness of testing procedure and that the Instron machine was working as expected. Cross head speed of 1.3 mm/min

was used in the tensile test and 10 data points were capture per second. The load cell of the Instron machine used in the tensile test has a maximum capacity of h 25 kN. After testing of the first three aluminum specimens, the stress strain curves were plotted and observed to agree with results found in the literature for the same material. Subsequently, the horizontally printed samples were tested using the same parameters.

A Split-Hopkinson Pressure Bar apparatus was used for the impact testing. The impact tests were performed on cylindrical specimen, 9.5 mm in diameter and 10.5 mm long. The impact specimens were deformed at strain rates of 150/s, 800/s, and 1300/s. Impact tests at each strain rates were repeated thrice and the reported stress and strain values are average of the values obtained from the three tests for each testing condition. A more detailed information on the test procedure and data analysis provided elsewhere in the literature (Tiamiyu, 2015).

RESULTS AND DISCUSSION

Microscopy

Melt Pool and Scanning

Cubic specimens of the AlSi10Mg-200°C were polished and etched to reveal the microstructure of the additively manufactured aluminum alloy samples. Microscopy was carried out on the surfaces parallel (side plane) and perpendicular (top plane) to the printing direction as shown in Figure 2.

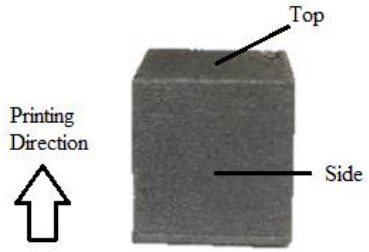

Figure 2. Cube sample with reference points for microscopy

Optical micrographs of polished and etched surfaces parallel and perpendicular to the 3D printing directions are presented in Figure 3. In the microstructure of the surface parallel to printing direction (Figure 3a), the melt pools as material was melted layer by layer to form the part are visible. The microstructure of the surface perpendicular to printing direction (Figure 3b) shows the scanning direction as the laser travels back and forth across each layer following the predetermined scanning strategy.

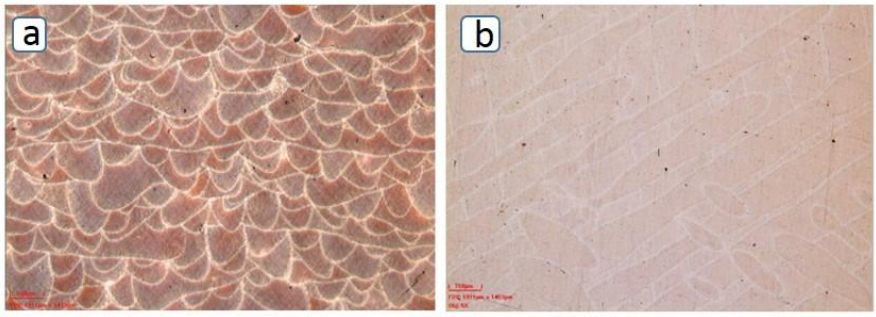

Figure 3. Typical micrographs of polished surface (a) parallel and (b) perpendicular to 3D printing direction

By applying a 1µ finish and using Keller's reagent during metallographic preparations, it is possible to clearly see the melt pools on planes parallel to the 3D printing direction (Figure 3a), which were created during processing. It can be observed that the material, once heated, sinks downwards to create these pools along each layer. The scanning strategy can be observed on the surface perpendicular to the 3D printing direction (Figure 3b) where there appears to be two visible layers along the diagonal of the rectangular micrograph that are perpendicular to one another

Tensile Test Results

The horizontally printed samples were tested and the resulting stress-strain curves are shown below in Figure 4.

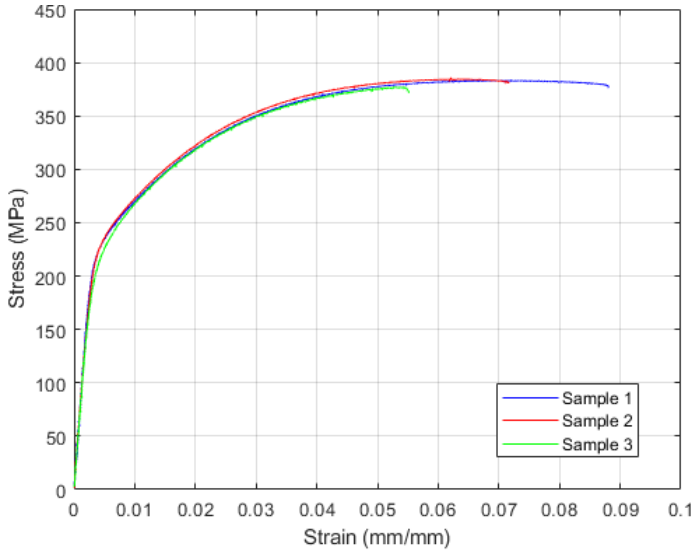

Figure 4. Stress vs. strain for horizontally printed AlSi10Mg-200°C samples

As shown above, the curves are extremely consistent seeming to confirm that additively manufactured parts using DMLS technique can demonstrate consistent mechanical properties from part to part. The modulus of elasticity was estimated to be 70 GPa, while the 0.2% offset yield stress was determined to be 235 MPa. The ultimate tensile strength is 386 MPa. The elongation to fracture of the specimens vary slightly from sample to sample and it is within the range 5.5% to 8.8%.

Comparison

Table 3 provides a comparison of the mechanical properties the horizontally printed AlSi10Mg-200°C samples and those of die-cast A360.

Table 3. Comparison of mechanical properties of AlSi10Mg-200°C and A360.0 die-cast

	AlSi10Mg_200C (Horizontal)	A360 (Die-Cast)
Ultimate Tensile Strength (MPa)	386	317
Yield Strength (MPa)	240	165
Elongation (%)	5.5–8.8%	3.50%
Modulus of Elasticity (GPa)	70	71

It can be seen that horizontally printed AlSi10Mg_200C has a higher elongation to fracture, yield strength, and modulus of elasticity than A360 die-cast. It is very likely that the trend will be the same for vertically printed samples. This is because the layers during the additive process are layered vertically in

the z-direction. For a horizontal specimen there would be less layers and during the tensile test the force would not pull these layers apart. During a tensile test for the vertical specimen, the force is acting normal to the layers resulting in the layers being pulled apart from each other. This suggests that vertically printed samples might even have higher strength than the horizontally printed specimens. The die-cast material shows a much lower strength, yield strength and elongation at break compared to the additively printed material.

Impact Test

The dynamic stress-strain curves obtained from impact test at strain rates of 150 /s, 800 /s, and 1300 /s are provided in Figure 5.

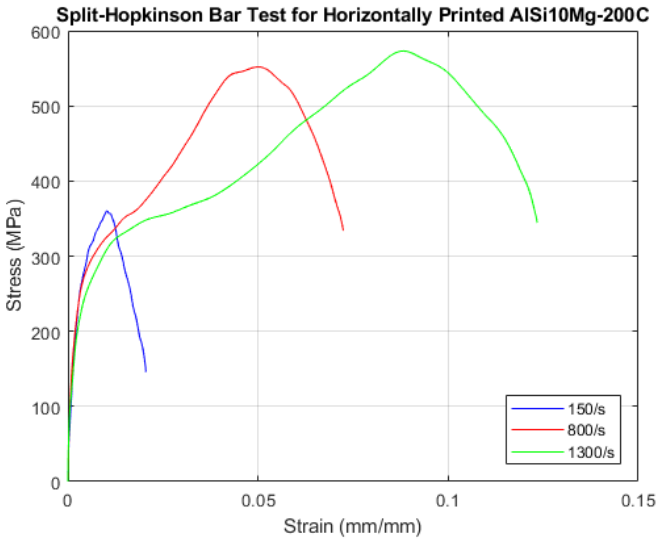

Figure 5. Dynamic stress strain curves of 3D printed AlSi10Mg alloy obtained from dynamic impact test using SHPB.

Each of the presented stress-strain curves is averaged from three samples tested at their respective strain rates. It can be seen from above that all three strain rates deform elastically at the beginning similarly as the curves are directly on top of each other until approximately 200 MPa. For 150/s the maximum stress is 360 MPa while total strain of the specimen is 1.8%. The maximum stress increased to 550 MPa when the strain rate was increased to 800/s, while the corresponding total strain of the specimen increased to 6.8%. When strain rate was further increased from 800 to 1300 /s, a slight increase in strength to 573 MPa was observed while substantial increase in total strain to 11.8% was recorded. .

For specimens deformed at 150/s, stress increases rapidly with strain until maximum stress is attained, when thermal softening began to dominate and stress falls. Deformation is governed predominantly by strain hardening until maximum stress is attained at this strain rate. The trend of the stress-strain curves when the specimens were impacted at 800/s and 1300/s are different from that of the specimens deformed at 150 /s. The curves samples deformed at 800 and 1300 /s experience a decrease in the rate of change of stress with strain in the 300–400 MPa stress range. This implies decrease in strain hardening rate attributable to initial thermal softening as the temperature of the specimen increased due to conversion of impact energy to thermal energy. Thereafter the strain hardening began to play domineering role on the deformation process due to work hardening (dislocation multiplication). Asgari et al. (2018) observed similar behaviour in magnesium alloys deformed at high strain rates and attributed the behaviour to strain hardening initially dominating plastic deformation followed by thermal softening and then a secondary strain hardening process (Asgari, 2018).

Constitutive Modelling

Tensile Test

A constitutive model is needed to successfully describe the findings of the tensile test. First the collected data from experiments was converted into graphs of stress vs. plastic strain. To accurately model the plastic region of the stress strain curve to provide future simulations with data points after the yield point, a hardening law is needed to be used. After trying various hardening laws, the Chang-Asaro Law was found to be a good fit and was eventually chosen and is shown below:

$$\sigma = \sigma_0 + Atanh(B\varepsilon^P) + C\varepsilon^P \quad (1)$$

where σ_0 is the yield stress, ε^P is the plastic strain, and A,B,C are constants. The horizontal stress plastic strain curve was fit as shown below in Figure 6.

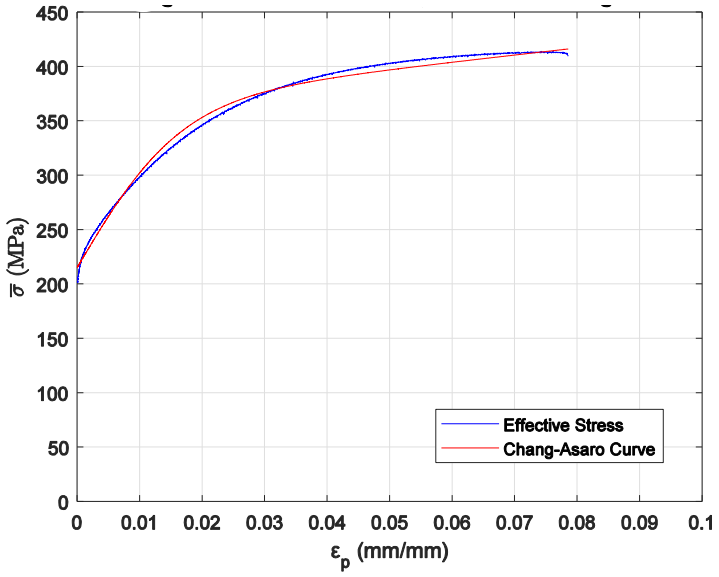

Figure 6. The Chang-Asaro curve fit for the horizontally printed tensile test

Impact Test

For future simulations it is more than likely that a constitutive model for a tensile test at a low strain rate will not be the only model needed to accurately depict the mechanical behaviour of parts made by horizontally printing of AlSi10Mg_200C, so a constitutive model was also developed for the impact testing shown below in Equation 2.

$$\bar{\sigma} = \sigma_0 + K\varepsilon_p^n \cdot \left[tanh^2\left(\frac{\varepsilon_p - \varepsilon_m}{A}\right) + B\right]\left[1 - \exp\left(C\frac{(\varepsilon_p - \varepsilon_f)}{\varepsilon_p}\right)\right] \quad (2)$$

The first part of the model is the yield stress, denoted by σ_0. The next portion of the equation mimics the power law hardening curve with strength coefficient *K* and hardening exponent *n* and manipulates the first part of the curve where the initial hardening and consequent softening occurs. The next portion of the curve relates to the "trough" observed between the two peaks at higher strain rates. While *A* controls the width of said trough, ε_m relates to the location of the local minima and *B* controls the depth. The third part of the model considers the end of the curve where the secondary hardening peak occurs and consequent secondary softening. For this portion *C* depicts the degree of curvature of this section while ε_f decides relates to where the failure strain will be. The constants described are shown for each of the strain rates in Table 4.

Table 4. Constants for varying strain rates

Parameter	150 /s	800 /s	1300 /s
K	4	808	541
n	0.7	0.7	0.35
A	0.001	0.012	0.05
ε_m	0.03	0.015	0.021
B	1000	3.03	1.11
C	1.20	2.75	3.60
ε_f	0.012	0.072	0.13
σ_0	270	250	200

It is apparent with the above table that the yield stress (σ_0) appears to decrease with increasing strain rate. The parameter ε_f increases along with strain rate as expected as it relates to the total strain. This model was fitted to the impact results from each of the three tested strain rates as shown below in Figure 7.

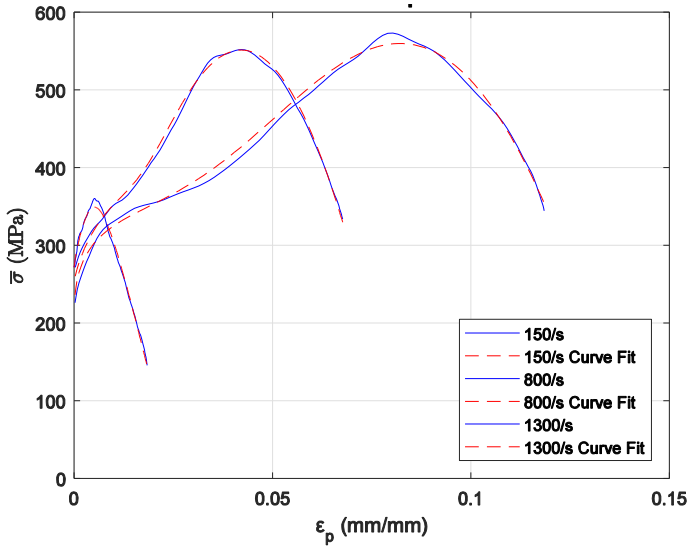

Figure 7. The resulting curve fits for the impact testing at various strain rates

The model shows its capabilities in Figure 7 as each of the strain rates is matched adequately by the model with little separation at any point on the curve. Although the results shown do not exceed a strain rate of 1300/s, this model could still be used at higher strain rates with the manipulation of constants previously mentioned in Table 4.

CONCLUSIONS

The horizontally printed AlSi10Mg-200°C samples during additive manufacture of this alloy were tested and the properties compared with those of A360.0 die-cast alloy. The additively manufactured samples displayed a higher yield strength, ultimate tensile strength and elongation to fracture compared to the die-cast A360.0 alloy. Constitutive models were than chosen for both tensile results as well as impact results for future use in simulations. The Chang-Asaro law was found to accurately fit the tensile tests but for the impact testing an existing model was not found. This led to the development of a new model used which adequately encompasses the multiple hardening and softening regions seen in the impact test results. Tensile tests also showed that there was very little fluctuation between the obtained curves for different samples, indicating consistency in mechanical data for additively manufactured metallic alloys.

ACKNOWLEDGMENTS

The authors would like to thank Natural Sciences and Engineering Research Council of Canada (NSERC)-RGPIN-2016-04221 and New Brunswick Innovation Foundation (NBIF)- RAI 2016-108 for providing sufficient funding to execute this work. They would like to thank UNB mechanical technicians, Brian Guidry, Bob MacAllister, and Vince Boardman. Finally, the authors greatly thank Additive Metal Manufacturing (AMM) in Concord, Ontario for designing, preparing, and providing additively manufactured samples to complete this work.

REFERENCES

Asgari, A. O. (2018). On dynamic mechanical behavior of additively manufactured. *Elsevier*.

Carter, L., Martin, C., Withers, P., & Attallah, M. (2013). The influence of the laser scan strategy on grain structure and cracking behaviour in SLM powder-bed fabricated nickel superalloy. *Journal of Alloys and Compounds, 615*, 338-339.

E8/E8m - 15a Standard Test Methods for Tensions Testing of Metallic Materials. (2015). ASTM.

Frazier, W. (2014). Metal Additive Manufacturing: A Review. *Journal of Materials Engineering and Performance, 23*(6), 1918-1919.

Gu, D., Meiners, W., Wissenbach, K., & Poprawe, R. (2013). Laser additive manufacturing of metallic components: materials, processes and mechanisms. *International Material Reviews, 57*(3), 133-134.

Herderick, E. (2011). Additive manufacturing of metals: A review. *Additive Manufacturing of Metals*, 1413-1414.

Herzog, D., Seyda, V., Wycisk, E., & Emmelmann, C. (2016). Additive manufacturing of metals. *Acta Materialia, 117*, 372-373.

Manfredi, D., Calignano, F., Krishnan, M., Canali, R., Ambrosio, E., & Atzeni, E. (2013). From Powders to Dense Metal Parts: Characterization of a Commercial AlSiMg Alloy Processed through Direct Metal Laser Sintering. *Materials, 6*, 860.

Metal Solutions. (2014). The Additive Manufacturing System for the Production of Serial Components, Spare Parts and Functional Prototypes Directly in Metal. EOS.

Murr, L., Gaytan, S., D. Ramirez, E. M., Hernandez, J., Amato, K., Shindo, P., . . . Wicker, R. (2012). Metal fabrication by additive manufacturing using laser and electron beam melting technologies. *Elsevier, 28*, 304.

Thijs, L., Kempen, K., Kruth, J.-P., & Humbeeck, J. V. (2012). Fine-structured aluminium products with controllable texture by selective laser melting of pre-alloyed AlSi10Mg powder. *Acta Materialia*, 1809-1811.

Tiamiyu, R. B. (2015). Plastic deformation in relation to microstructure and texture evolution in AA 2017-T451 and AA 2624-T351 aluminum alloys under dynamic impact loading. *Materials Science & Engineering A*.

Zinoviev, A., Zinovieva, O., Ploshikhin, V., Roimanova, V., & Balokhonov, R. (2016). Evolution of grain structure during laser additive manufacturing. Simulation by a cellular automata method. *Materials and Design, 106*, 321-322.